Driving Forces for Adsorption of Polyols onto Zeolites from Aqueous Solutions

Elizabeth E. Mallon, Aditya Bhan,* and Michael Tsapatsis*

University of Minnesota, Department of Chemical Engineering and Materials Science, 421 Washington Avenue SE, Minneapolis, Minnesota 55455

Received: November 4, 2009; Revised Manuscript Received: December 18, 2009

Ambient temperature adsorption isotherms have been developed for C_2-C_6 diols and triols on small (FER), medium (MWW, MFI, BEA), and large (MOR, FAU) pore zeolites as well as on ordered mesoporous materials (MCM-36, 3DOm-MFI, and SBA-15) using gravimetry. Henry's constants for diol and triol adsorption on silicalite-1 increase exponentially with carbon number demonstrating that confinement of the adsorbate in the zeolite pores is the primary driving force for adsorption. This conclusion is supported by results for propylene glycol adsorption at low coverages on materials differing in topology and chemical composition. It is shown that adsorption decreases with an increase in the adsorbent pore size, and aluminum content only has a marginal effect. Comparison of diol and triol adsorption on silicalite-1 shows that increasing the number of hydroxyl groups causes a decrease in the Henry's constant possibly due to a change of the configuration of the adsorbate in the zeolite pores, while the location of the hydroxyl groups does not have a significant effect. Overall, this study provides evidence that polyol adsorption is primarily a function of dispersion forces that are derived from the fit of the adsorbate in the adsorbent pores. These findings could have an impact on the separation and catalytic conversion of oxygenates in the processing of biomass to chemicals and fuels.

Introduction

Coal, natural gas, and crude oil are used to produce approximately 95% of the carbon-containing commodity chemicals, but many of these chemicals can also be manufactured from plant-based carbohydrates, lipids, and oils.[1] Propylene glycol, 1,3-propanediol, and ethylene glycol are diols, hydrocarbons functionalized with two hydroxyl (−OH) groups, which constitute some of the commodity chemicals that can be produced from fossil and renewable feedstocks. Fermentation is a potential route for obtaining diols from biomass, but to separate species in the reactor effluent using a traditional separation process, pretreatment of the effluent stream to remove unreacted sugars and proteins is required since these molecules are thermally sensitive and nonvolatile.[2] Furthermore, the target product has a low vapor pressure, so a distillation step would be used to remove water, the primary component, resulting in an energy intensive and expensive unit operation which may account for 50−70% of the total production cost.[3,4] A membrane or adsorption separation process may be able to replace one or more of these separation steps, making production of diols using renewable feedstocks a viable synthetic route. Zeolitic materials are potential candidates in this application due to their high pressure and temperature stability, selectivity, and flux.[5]

The ability of zeolites to discriminate alkanes of varying length and degree of branching has already made their use prevalent in petrochemical processes such as fluid catalytic cracking,[6] isomerization,[7] and alkylation.[8,9] Earlier studies have identified that alkane adsorption in zeolites is predominantly a function of three interactions: van der Waals forces between the zeolite pore and the adsorbate, electrostatic interactions between the adsorbate and Brønsted acid sites, and adsorbate−adsorbate interactions. It has been shown that the fit between the alkane and zeolite pore has the most significant effect on the enthalpy and entropy of alkane adsorption.[10–15] Theoretical and experimental studies have shown that Henry's constant, K_{ads}, increases exponentially with *n*- and iso-alkane carbon number for several zeolite frameworks including MFI,[10,12,16] MOR,[12,13,16] FAU,[10,12,13,15] FER,[11,15] TON,[15] MTW,[15] UTD-1,[15] MWW,[14] and BEA[13,16] due to an increase in dispersion forces with each additional carbon.

Since dispersion forces are a function of the fit between the adsorbate and zeolite, it was found by Eder et al. using calorimetry and gravimetry that the heat of adsorption of *n*- and iso-alkanes decreases in the sequence H-MFI > H-MOR > H-FAU correlating with an increase in pore size.[12] This trend was confirmed by Savitz et al. who used a Lennard−Jones 12-6 potential to calculate the heat of adsorption and Henry's constant for methane adsorption in pure silica analogues of the FER, TON, MFI, MTW, UTD-1, and FAU frameworks.[15] The authors obtained an average error of 8% for the enthalpies and 29% for the Henry's constants between the simulated and experimental results indicating again that confinement effects are the dominant contributor to the energy of adsorption for *n*-paraffins.

While extensive experimental and theoretical studies have led to well-defined structure−property correlations for the adsorption of linear and branched alkanes on zeolites, analogous relationships for the adsorption of oxygenated molecules have yet to be fully developed. Studies have shown that methanol adsorption is a function of both electrostatic interactions with Brønsted acid sites and van der Waals interactions with the pore walls. Ison and Gorte used gravimetric and spectroscopic techniques to show at an adsorbate pressure of 80 Torr on H-ZSM-5 at ambient conditions that methanol hydrogen bonds with the Brønsted acid site protons and with other methanol molecules thereby forming clusters.[17] Other studies confirmed this result, indicating that electrostatic interactions between Brønsted acid sites and the methanol −OH group control the

* Corresponding authors. Phone: 612-626-3981 (Bhan), 612-626-0920 (Tsapatsis). Fax: (612) 626-7246. E-mail: abhan@umn.edu and tsapatsi@cems.umn.edu.

10.1021/jp910543r
Published on Web 01/13/2010

location of the adsorbate within the zeolite structure.[18,19] The chemical makeup of the zeolite was shown to not only control the location of adsorbed methanol in MFI pores but also have a substantial affect on the heat of adsorption of C_1-C_3 alcohols using calorimetry. For all alcohols studied, the heat of adsorption for coverages less than 400 μmol g^{-1} increased by 50−60 kJ mol^{-1} from silicalite-1 to H-ZSM-5.[20] Although the chemical composition was demonstrated to contribute to the enthalpy of adsorption, confinement was also shown to have a significant effect; the heat of adsorption increased 15−20 kJ/mol for each additional carbon irrespective of aluminum content.[20]

Diol adsorption and permeation experiments have given some insight to the interactions that control adsorption for this class of oxygenates. Long et al. performed a gravimetric study of oxygenated molecules on pure silica MFI.[21] The authors noted that glycerol, propylene glycol, and 1,3-propanediol have similar molecular volumes, but the maximum volume of glycerol adsorbed at saturation was 1 order of magnitude less than the diols which they attributed to an increase in hydrophilicity from the addition of a third hydroxyl group. Li et. al have reported results for pervaporation experiments with binary, ternary, and quaternary feeds of 1,3-propanediol, glycerol, glucose, and water across a variety of zeolite membranes at temperatures ranging from 308 to 328 K.[22–25] It was reported on the basis of these studies that 1,3-propanediol/water separation selectivities for all zeolite membranes were higher than the ratio of their volatilities (0.038) leading to the conclusion that interactions between 1,3-propanediol and water with the membrane are significant.[23] The authors found that 1,3-propanediol selectivity was greater than 1 only for siliceous (Si/Al > 600) zeolites and that the highest selectivity was achieved with silicalite-1. It was also noted that the 1,3-propanediol permeate concentration was greater with silicalite-1 than with ZSM-5 (Si/Al = 25) which led the authors to conclude that the removal of Brønsted acid sites creates a more hydrophobic surface which facilitates 1,3-propanediol transport through the zeolite pores.[23]

While the aforementioned reports in the literature discuss single-component adsorption of diols on zeolites at saturation loading and the permeation of polyols (hydrocarbons with multiple −OH groups) through zeolite membranes, no relationship between K_{ads} and chemical functionality of the adsorbate has been determined for polyol adsorption on zeolites. The aim of the results and analysis presented herein is to determine structure−property correlations for the adsorption of polyols on zeolites using gravimetry. Specifically, C_2-C_6 diol and triol adsorbates were used in these experiments to isolate the effects of carbon number and functionality on polyol adsorption. In addition, several zeolite frameworks and ordered mesoporous materials with varying Al content were selected as adsorbents to determine the effect of topology and chemical composition on polyol adsorption. We report that K_{ads} increases exponentially with carbon number for C_2-C_6 diols and triols due to an increase in dispersion forces. Our results also show that K_{ads} increases with decreasing pore size and is only weakly dependent on the number of Brønsted acid sites within the range studied emphasizing the dominant role of confinement for polyol adsorption.

Experimental Section

Materials. All experiments were performed with protonated forms of the different zeolite frameworks. The Si/Al ratio for all zeolite adsorbents used in this study is presented in Table 1. FER, MFI, BEA, MOR, and FAU zeolites of varying aluminum content were procured in either their protonated or ammonium form from Zeolyst. Silicalite-1[26] and ITQ-1,[27] pure silica analogues of the MFI and MWW frameworks, respectively, were synthesized using previously reported procedures. SBA-15 was synthesized using the 2 day aging procedure reported by Kruk et al.[28] 3DOm-MFI with a mesopore size of 10 nm was synthesized using the procedure developed by Fan et al.[29] and a ZSM-5 synthesis solution (Si/Al = 50) prepared according to the method reported by Schmidt et al.[30] MCM-22(P) was synthesized in the Na^+ form according to the procedure used by Maheshwari et al.; MCM-36 was then obtained using room-temperature swelling of MCM-22(P) as described by the authors.[31] This version of MCM-36 exhibits a high degree of structural preservation of the microporous layers compared to previously reported MCM-36 materials. The NH_4^+ form of MCM-22 was obtained via ion exchange with 1 N NH_4NO_3 at ambient conditions for 24 h.[32] X-ray diffraction was used to confirm the structural integrity of all zeolite adsorbents. Zeolite samples (∼1.5 g) were treated under flowing dry air (Minneapolis Oxygen Industrial, Compressed Industrial Air; 1.67 cm^3 s^{-1}) from ambient temperature to 823 K at a rate of 0.2 K s^{-1}, holding at 823 K for 10 h, and subsequently cooling to ambient temperature.

TABLE 1: Chemical Composition of Adsorbents

zeolite name	framework	source	Si/Al	Al/uc
CP914	FER	Zeolyst	29[a]	1.2
ITQ-1	MWW	Synthesis	∞	0
MCM-22	MWW	Synthesis	47	1.5
CBV2314	MFI	Zeolyst	13[a]	6.8
CBV8014	MFI	Zeolyst	43[a]	2.2
CBV28014	MFI	Zeolyst	140	0.7
silicalite-1	MFI	Synthesis	∞	0
CP814E	BEA	Zeolyst	12	4.9
CP811E-75	BEA	Zeolyst	48	1.3
CP811C-300	BEA	Zeolyst	100	0.6
CBV21A	MOR	Zeolyst	11[a]	4.0
CBV90A	MOR	Zeolyst	44[a]	1.1
CBV720	FAU	Zeolyst	15	12
CBV760	FAU	Zeolyst	30	6.2
3DOm-MFI	MFI/Meso	Synthesis	50	-
MCM-36	MWW/Meso	Synthesis	47	-
SBA-15	Micro/Meso	Synthesis	∞	0

[a] Si/Al determined using inductively coupled plasma−optical emission spectroscopy by Galbraith. All other Si/Al values from Zeolyst or approximated from synthesis procedure.

The adsorbates used for all results presented were in the liquid phase at ambient temperature and atmospheric pressure. Aqueous solutions with a volume of 1 mL and concentrations ranging from 1 to 25 μmol mL^{-1} were prepared in closed glass vials. Approximately 100 mg of zeolite adsorbent was added to each vial, and the zeolite−solution mixtures were stirred at 1200 rpm and ambient temperature until equilibration. Each solution was filtered with a 3 mL Monoject syringe fitted with a 0.2 μm GHP (polypropylene) syringe filter to remove the zeolite particles, and the filtrate was prepared for analysis with liquid chromatography.

Chromatography. The filtrate concentrations were analyzed using an Agilent 1200 High Performance Liquid Chromatography (HPLC) system equipped with a refractive index detector (RID) and an autosampler. The autosampler removed 20 μL of sample from a single vial and injected the contents into a stream of 0.005 M sulfuric acid (H_2SO_4) in deionized water with a flow rate of 0.008 mL s^{-1}. The stream was passed through a Bio-Rad Aminex HPX-87H polystyrene packed column heated to 333 K at the inlet and 318 K at the outlet, and the column pressure was maintained at 40−60 bar. The outlet stream was passed through a refractive index detector (RID) which was

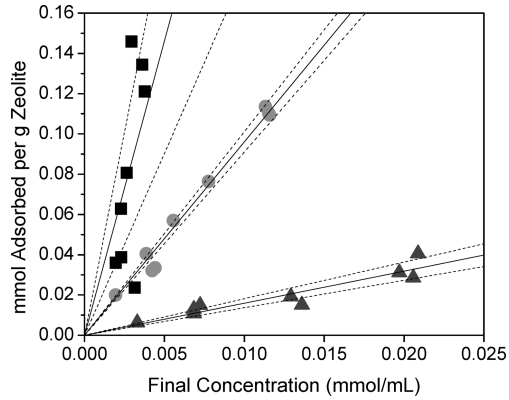

Figure 1. Adsorption isotherms at 298 K for 1,2-butanediol (■), propylene glycol (●), and ethylene glycol (▲) on MFI silicliate-1. Solid lines are from unweighted least-squares linear regressions. Dashed lines represent 95% confidence intervals.

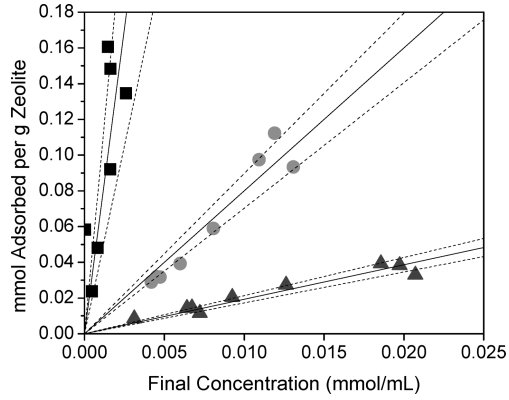

Figure 2. Adsorption isotherms at 298 K for 1,2-butanediol (■), propylene glycol (●), and ethylene glycol (▲) on BEA CP811C-300. Solid lines are from unweighted least-squares linear regressions. Dashed lines represent 95% confidence intervals.

heated to 323 K. The RID signal output was recorded and plotted against time, and the adsorbate peak was identified from the retention time. The relative signal intensities of the adsorbate and a glycerol or propylene glycol internal standard were used to determine the final concentration of each solution. The difference in the initial and final concentration of the adsorbate and the total volume of the solution was used to calculate the uptake of the adsorbate.

Results and Discussion

Confinement Effects. The adsorption isotherms for ethylene glycol, propylene glycol, and 1,2-butanediol in water on high Si/Al forms ($47 < Si/Al < \infty$) of the MFI, BEA, and MWW frameworks are shown in Figures 1−3. The amount adsorbed increases with increasing carbon number for MFI, BEA, and MWW which implies that confinement effects adsorption uptake at low diol loadings.

This hypothesis was further probed via analysis of the partition coefficients between the bulk and adsorbed phases (K_{ads}) for these systems. Values of K_{ads} were extracted from the adsorption isotherm data presented based on the following assumptions: it has been shown through gravimetric measurements that water adsorbs in MFI pores only at Brønsted acid sites[18,33,34] and at the silanol groups that arise at the external crystal surface and crystal defects.[20,35] Furthermore, on the basis of single and binary component adsorption studies done using gravimetry, calorimetry, and FTIR spectroscopy, it was shown

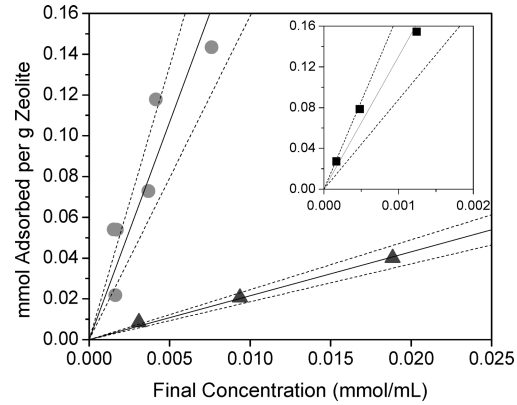

Figure 3. Adsorption isotherms at 298 K for 1,2-butanediol (■), propylene glycol (●), and ethylene glycol (▲) on MWW MCM-22. Solid lines are from unweighted least-squares linear regressions. Dashed lines represent 95% confidence intervals.

that water adsorbs with a heat of adsorption of approximately 30 kJ mol^{-1} less than methanol,[20] and when methanol and water are co-fed onto a zeolite, methanol will displace water at Brønsted acid sites.[17] Upon the basis of these experimental observations reported in the literature, we assumed in our analysis that water−zeolite interactions are negligible. The solution concentrations used in these experiments (1−25 μmol mL^{-1}) are in the infinitely dilute regime where the activity coefficients are approximately equal to unity.[36] Therefore, water−adsorbate interactions were also neglected, and the adsorption isotherms presented herein were treated as single-component isotherms. Due to these assumptions, the partition coefficients will be referred to as Henry's constants from this point forward.

It should also be noted that coverages for all data reported were below 4 molecules per unit cell (~0.001 to 1 molecules per unit cell and less than 10% of the total micropore volume) which corresponds with an inflection in the isotherms for hexane, heptane, and C_4−C_7 2-methyl branched alkane adsorption in silicalite-1.[37,38] Smit and Maesen used configurational-bias Monte Carlo (CBMC) simulations to show that the inflection point in hexane and heptane isotherms was due to "commensurate freezing".[37] Similarly, the inflection in the adsorption isotherm for C_4−C_7 2-methyl branched alkane adsorption in silicalite-1 was attributed to preferential adsorption of these bulkier molecules in the channel intersections at low pressures and that adsorption in the pores, the secondary adsorption site, only occurs when adequate pressure in the bulk phase is achieved.[38] While isotherms with inflection points are typically modeled as dual-site Langmuir isotherms and it is unknown if polyol adsorption isotherms contain this feature since full isotherms have not been obtained, the isotherms presented herein are for low pressures when it is likely that the adsorbate molecules occupy one preferred adsorption site and were therefore modeled as single-component single-site Langmuir isotherms. The data were then fit using least-squares linear regression, and values for K_{ads} were determined from the slopes of the lines.

An exponential increase in K_{ads} with 1,2-diol carbon number on silicate-1, BEA, and MWW was noted (Figure 4) implying that the free energy of adsorption, ΔG_{ads}, increases linearly with carbon number for C_2−C_4 diols. As with alkane adsorption, this result implies that the energy of adsorption for diols increases by a fixed amount with each additional carbon, and therefore dispersion forces are critical for diol adsorption.

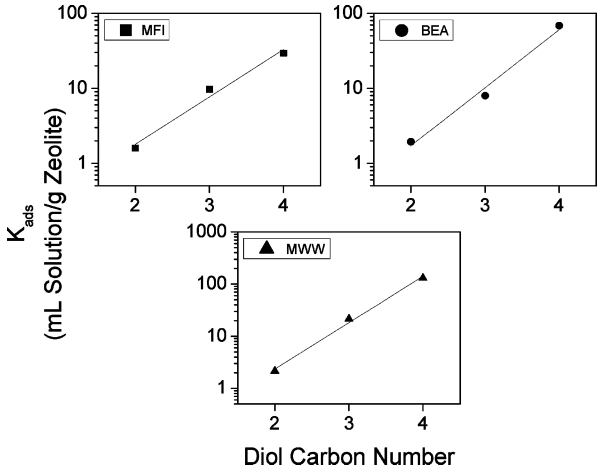

Figure 4. K_{ads} versus 1,2-diol carbon number for MFI silicalite-1, BEA CP811C-300, and MWW MCM-22 at 298 K. Solid lines are from unweighted least-squares linear regressions.

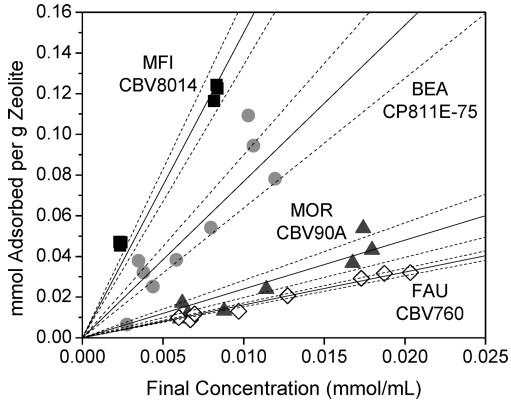

Figure 5. Adsorption isotherms at 298 K for propylene glycol on MFI (■), BEA (●), MOR (▲), and FAU (◊) with Si/Al∼40. Solid lines are from unweighted least-squares linear regressions. Dashed lines represent 95% confidence intervals.

Since confinement is a function of the fit between the adsorbate and the zeolite pores, the dependency of K_{ads} for propylene glycol adsorption on the material topology was explored. Note that propylene glycol was chosen as the probe molecule since it is a current commodity chemical as well as an appropriate surrogate compound for biomass due to its similar chemical functionality. Solutions of propylene glycol and water were adsorbed on different Si/Al ratios of the MFI, BEA, MOR, and FAU frameworks. The adsorption isotherms are grouped by Si/Al∼10 and Si/Al∼40 and are presented in Figures 5 and 6. Since the aluminum content per unit cell is comparable for the frameworks as shown in Table 1, these data demonstrate that the framework geometry has a strong effect on the amount of propylene glycol adsorbed.

Adsorption isotherms for propylene glycol on mesoporous materials MCM-36, 3DOm-MFI, and SBA-15 are shown in Figure 7. These are compared with the adsorption isotherms for the pure silica analogue of MWW, ITQ-1, and MFI CBV28014 (Si/Al∼140). It can be observed that MCM-36, which has the MWW micropore structure and 4.2 nm mesopores from silica pillaring between layers, and ITQ-1 have similar adsorption uptake at low concentrations of propylene glycol in water; the same relationship is apparent for propylene glycol adsorption in 3DOm-MFI (MFI micropores and 10 nm mesopores) and MFI. This indicates that propylene glycol preferentially adsorbs in the micropores of these materials.

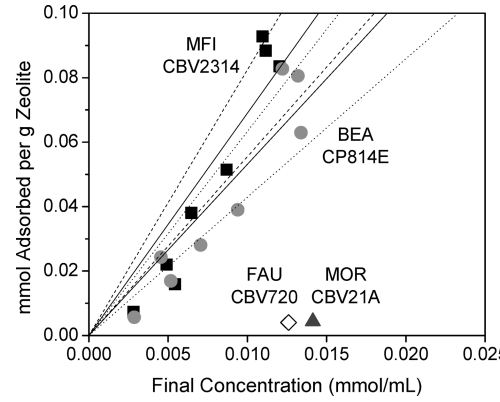

Figure 6. Adsorption isotherms at 298 K for propylene glycol on MFI (■), BEA (●), MOR (▲), and FAU (◊) with Si/Al∼10. Data points for FAU and MOR represent average values. Solid lines are from unweighted least-squares linear regressions. Dashed lines represent the 95% confidence interval for MFI. Dotted lines represent the 95% confidence interval for BEA.

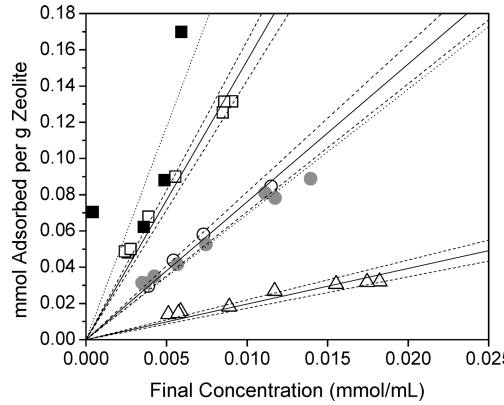

Figure 7. Adsorption isotherms at 298 K for propylene glycol on mesoporous materials MCM-36 (□), 3DOm-MFI (○), and SBA-15 (Δ) and on ITQ-1 (■), the pure silica analogue of MWW, and MFI CBV28014 (●). Solid lines are from unweighted least-squares linear regressions for the mesoporous materials. Dotted lines are unweighted least-squares linear regressions for ITQ-1 and MFI. Dashed lines represent 95% confidence intervals for the mesoporous materials.

K_{ads} values for propylene glycol adsorption on all Si/Al forms of the MWW, MFI, BEA, MOR, and FAU zeolite frameworks as well as the mesoporous materials MCM-36, 3DOm-MFI, and SBA-15 are plotted in Figure 8. The minimum accessible pore diameters were estimated from the unit cell structure of MWW, MFI, BEA, and FAU as reported by the International Zeolite Association.[39] Since it has been observed that straight alkanes with a carbon number greater than 4 preferentially adsorb in the 12 MR of MOR at saturation conditions,[40] it was assumed that the 8 MR ring pockets are inaccessible to propylene glycol, and therefore the minimum pore dimension for MOR was taken to be 6.5 Å. MCM-36 and 3DOm-MFI were assigned minimum pore sizes corresponding to MWW and MFI, respectively, since propylene glycol adsorption on these materials resulted in isotherms comparable to their zeolite counterparts as shown in Figure 7. SBA-15 synthesized in the aforementioned procedure[28] contains micropores with an average pore diameter of 17 Å, so this value was taken as the minimum pore diameter.[41,42]

It can be observed from the data reported in Figure 8 that K_{ads} decreases with increasing pore size for all zeolite frameworks and mesoporous materials explored. Taking into account the exponential dependence of K_{ads} on diol carbon number, it is likely that the decrease in K_{ads} with increasing pore size is caused by a decrease in dispersion forces.

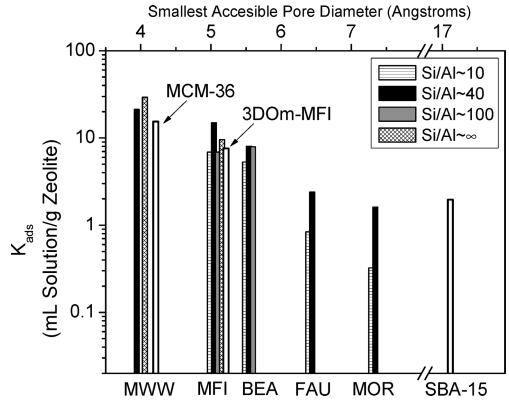

Figure 8. K_{ads} versus smallest accessible zeolite pore diameter for propylene glycol on the MWW, MFI, BEA, MOR, and FAU zeolite frameworks and mesoporous materials MCM-36, 3DOm-MFI, and SBA-15.

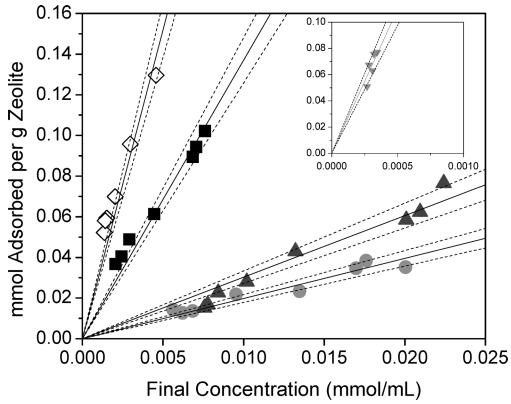

Figure 9. Adsorption isotherms at 298 K for 1,2-hexanediol (▼), 1,2-butanediol (■), propylene glycol (●), 1,3-propanediol (◊), and ethylene glycol (▲) on FER CP914. Solid lines are from unweighted least-squares linear regressions. Dashed lines represent 95% confidence intervals.

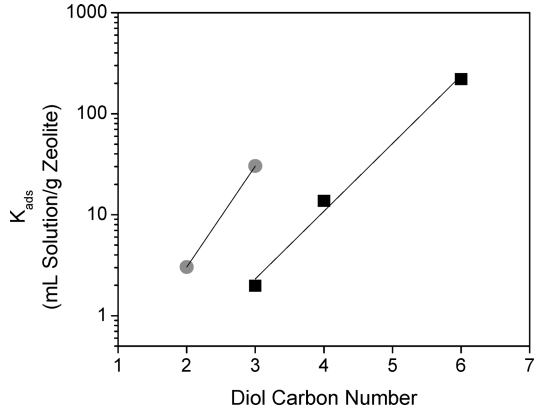

Figure 10. K_{ads} versus diol carbon number for 1,*n*-diols (●) and 1,2-diols with carbon number greater than 3 (■) on FER CP914 at 298 K. Solid lines are from unweighted least-squares linear regressions.

Shape Selectivity Effects. While it has been noted that diol adsorption increases with carbon number on silicalite-1, MWW, and BEA, this trend is not found with FER (Figure 9). In an effort to better understand the cause of this result, adsorption isotherms for 1,2-hexandiol and 1,3-propanediol on FER were developed as shown as in Figure 9. Values for K_{ads} were obtained using the procedure described previously and are compared in Figure 10. It can be observed that K_{ads} increases exponentially with carbon number for C_3-C_6 1,2-diols, but ethylene glycol has a higher K_{ads} than propylene glycol. Also, it is found that K_{ads} for 1,3-propanediol is 1 order of magnitude greater than propylene glycol (1,2-propanediol).

Similar trends have been identified for linear and dibranched alkane adsorption in FER.[40,43] ^{13}C NMR and FT-Raman studies have shown that linear alkanes with six or more carbon atoms cannot access the eight-membered ring channels of FER.[40] Pieterse et al. compared adsorption enthalpies between linear and dibranched alkanes in FER using gravimetry and calorimetry to find that the heat of adsorption decreases with an increase in branching.[43] The authors also noted using a combination of IR spectroscopic, gravimetric, calorimetric, and computational methods that the appended methyl groups inhibit the alkanes from fully entering the zeolite pores, and at coverages greater than 0.02 mmol per gram, 2,2-dimethylpentane and 2,2-dimethylhexane adsorb on the external crystal surface with the propyl and butyl groups pointing into the zeolite pores.[43] Since the data presented herein are for similar coverages (see Figure 9), it is hypothesized that adsorption of 1,2-diols with carbon numbers greater than 3 is hindered by the hydroxyl group on the secondary carbon, but the hydrocarbon chains of the C_3-C_6 1,2-diols can penetrate the pores of FER leading to the observed exponential dependence of K_{ads} on carbon number. Also, it is proposed that 1,3-propanediol can fully diffuse into the pores of FER leading to greater values for K_{ads} than 1,2-propanediol.

Effects of Brønsted Acid Sites. Henry's constants for propylene glycol adsorption on zeolites and mesoporous materials with varying aluminum content (Figure 8) can also be inspected to discern the effect of the framework chemical composition on propylene glycol adsorption. From these data, we note that a change in pore size from 4 to 7 Å results in a reduction of K_{ads} by an order of magnitude, but varying the aluminum content (and the synthesis method as shown in Table 1) results in an average standard deviation of less than 50% from the mean K_{ads} value for any given zeolite framework. This demonstrates that the fit between the adsorbate and zeolite pore is the most critical parameter for diol adsorption in zeolites at ambient temperature; the aluminum content for the range studied appears to only have a marginal effect.

A possible explanation for the weak dependence of K_{ads} on Si/Al ratio is a compensation effect. Eder et al. plotted the enthalpy of adsorption versus the entropy of adsorption for adsorption of C_3-C_6 *n*-alkanes on silicalite-1 and an aluminum-containing MFI zeolite.[10] A comparison of the points corresponding to hexane show that both the enthalpy and entropy of adsorption increase with an increase in aluminum content, leading to approximately the same value of K_{ads} for both frameworks. It is possible that a similar compensation effect is occurring for polyol adsorption resulting in only a small change in K_{ads} with Si/Al ratio.

Despite being a weak dependence, the trend of K_{ads} on the Si/Al ratio is clear: K_{ads} decreases with decreasing Si/Al ratio. It is possible that this decrease is from competitive adsorption with water, although the low aluminum content of the adsorbents (see Table 1) and the observation that water adsorbs with a heat of adsorption ~30 kJ mol^{-1} less than methanol[20] and is therefore displaced at Brønsted acid sites during coadsorption with methanol[17] indicate that this is unlikely to have a significant effect. Another possible cause of the decrease in K_{ads} with increasing aluminum content is partial blockage of the preferred adsorption sites of propylene glycol by the Brønsted acid site protons. Beerdsen et al. used configurational bias Monte Carlo (CBMC) simulations to identify that isobutane adsorption in MFI is inhibited by a decrease in Si/Al at pressures ranging from 10^{-3} to 10^5 kPa at 296 K.[44] Henry's constants calculated

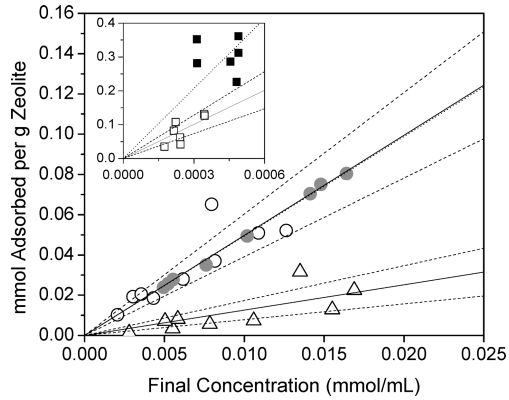

Figure 11. Adsorption isotherms at 298 K for 1,2,6-hexanetriol (□), 1,2,4-butanetriol (○), glycerol (Δ), 1,2-hexanediol (■), and 1,3-propanediol (●) on MFI silicliate-1. Solid lines are from unweighted least-squares linear regressions of the triols. Dotted lines are from unweighted least-squares linear regressions of the diols. Dashed lines represent 95% confidence intervals for the triols.

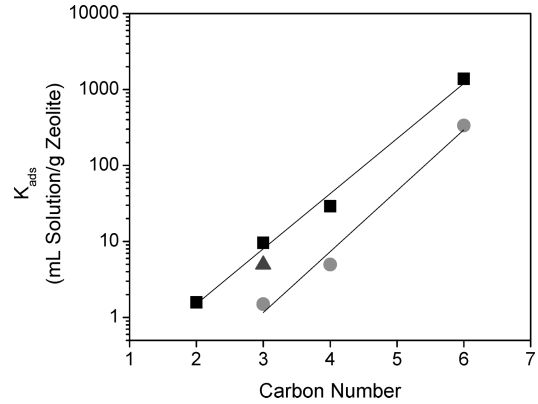

Figure 12. K_{ads} versus carbon number for 1,2-diols (■), 1,2,*n*-triols (●), and 1,3-propanediol (▲) on MFI silicalite-1 at 298 K. Solid lines are from unweighted least-squares linear regressions.

by the authors also decreased as Si/Al decreased for all nonframework cations (cations balancing negatively charged framework oxygens) studied. The authors concluded that the nonframework cations, which mainly reside at the channel intersections, inhibit isobutane from fitting into the channel intersections where it preferentially adsorbs at low pressures, thereby decreasing K_{ads}. It is possible that diols also adsorb preferentially at channel intersections due to the appended hydroxyl groups, and therefore a decrease in Si/Al would result in a decrease in the available adsorption sites at low concentrations and a concomitant decrease in K_{ads}.

Effects of Adsorbate Hydroxyl Groups. The adsorption isotherms for glycerol, 1,2,4-butanetriol, and 1,2,6-hexanetriol in water on silicalite-1 are shown in Figure 11. As with the 1,2-diols, the amount adsorbed increases with increasing carbon number reaffirming confinement as the primary driving force for adsorption. Also shown in Figure 11 are the adsorption isotherms for 1,2-hexanediol and 1,3-propanediol. It can be observed from the isotherms that there is a greater uptake of 1,2-hexanediol than 1,2,6-hexanetriol at low coverages. This indicates that the addition of an −OH group decreases the affinity for adsorption. It is also interesting to note that the adsorption isotherms of 1,3-propanediol and 1,2,4-butanetriol are collinear illustrating that increasing carbon number and decreasing hydroxyl number by the same amount may result in similar adsorption configurations in MFI.

A comparison of the K_{ads} values for propylene glycol (1,2-propanediol) and 1,3-propanediol in Figure 12 indicates that the location of the −OH groups does not have a significant effect on the strength of diol adsorption in silicalite-1. Upon the basis of this result, we postulate that C_3 diols have similar configurations within the zeolite pores at low coverages regardless of the location of the hydroxyl groups.

The adsorption isotherms for C_3, C_4, and C_6 triols on silicalite-1 were also analyzed as single-component single-site Langmuir isotherms allowing us to determine K_{ads}. A plot of K_{ads} versus carbon number for C_2−C_6 diols and triols shows that K_{ads} increases exponentially with carbon number for both classes of adsorbates (Figure 12) and that K_{ads} for any triol is lower than the value for the diol with a corresponding number of carbons. The change in K_{ads} with the addition of an −OH group indicates that diols and triols have different adsorption configurations within the pore network.

Differences in triol and diol configurations can be hypothesized from the trends observed for *n*- and iso-alkane adsorption on MFI.[11,16] Denayer et al. used the pulse chromatographic technique to measure equilibrium adsorption coverages and found that on MFI the Henry's constant for a given carbon number alkane decreased with increased branching.[16] This result indicates a change in the preferred configuration of alkanes with an increase in branching. This was confirmed via Monte Carlo simulations by June et al. who found that *n*-hexane adsorbs in the pores of silicalite-1 with a heat of adsorption of 68 kJ mol^{-1}, while 2- and 3-methyl pentane adsorb at the channel intersections with a 5 kJ mol^{-1} lower heat of adsorption.[45] The authors also found that K_{ads} values for methylpentanes are lower than those for *n*-hexane indicating that the configuration of the branched alkanes in the channel intersections results in weaker interactions with the pore walls. CBMC work performed by Smit et al.[46] confirmed the results of June et al. and identified that monomethyl branched alkanes with a carbon number of 5 and 6 will reside completely in the MFI channel intersections, whereas the branched alkanes with carbon numbers ranging from 7 to 10 will adsorb with the bulky headgroup in the channel intersection and the slender tails in the straight channel. Upon the basis of these results for alkane adsorption, we postulate that diols and triols may also arrange themselves with the branched groups in the pore intersections and the hydrocarbon tails in the channels. This hypothesis is supported by two major features of Figure 12—the decrease in K_{ads} from a diol to a triol with a corresponding number of carbons and the comparable increase in K_{ads} with carbon number for diols and triols. The decrease in K_{ads} from diols to triols could be caused by a decrease in the interactions with the pore walls from the addition of a hydroxyl group, while the increase of K_{ads} with carbon number could be caused by an increase in van der Waals interactions between the hydrocarbon chain and the zeolite channel walls.

It is also noteworthy that the lower value of K_{ads} for glycerol when compared with 1,2- and 1,3-propanediol corresponds well with the silicalite-1 adsorption results of Long et al. The authors found that the glycerol saturation coverage was an order of magnitude lower than that of the diols.[21] The results presented herein show that glycerol adsorption is less favorable than diol adsorption at low coverages, and this is likely due to a change in the preferential adsorption configuration due to hindrance from the third −OH group.

Our results also demonstrate that the high 1,3-propanediol/glycerol selectivity observed by Li et al. in the permeate feed may be partially due to the greater affinity of MFI for diol adsorption.[23] Our observation that K_{ads} decreases with a decrease in Si/Al also corroborates the result that 1,3-propanediol/water

selectivity was greatest with silicalite-1 and that the removal of Brønsted acid sites increases the affinity for diol adsorption.[23]

Conclusions

Liquid phase adsorption isotherms of diols and triols were analyzed with respect to the known primary influences on the adsorption of alkanes in zeolites at low coverages: adsorbate−zeolite interactions related to the confinement of the adsorbate in the zeolite pore and hydrogen bonding between the adsorbate and zeolite Brønsted acid sites.

The logarithm of Henry's constants increased monotonically with carbon number for diol and triol adsorbates irrespective of the chemical identity of the framework implying that dispersion forces are the primary factor for adsorption in zeolites. This conclusion was supported by the result that the Henry's constants for propylene glycol adsorption on different zeolite frameworks and mesoporous materials decrease with an increase in adsorbent pore size. Adsorption isotherms for diols on FER indicate that 1,2-diols with carbon numbers greater than 3 cannot diffuse into the zeolite pore network and are likely adsorbed on the external crystal surface with the long hydrocarbon tail confined in the zeolite pore. Henry's constants for triol adsorption on silicalite-1 were systematically lower than diols of the same carbon number leading to the hypothesis that the addition of −OH groups hinders interactions with the zeolite pore wall, whereas K_{ads} for 1,2- and 1,3-propanediol adsorption on silicalite-1 was approximately the same indicating that the location of the −OH does not significantly change the diol configuration in the zeolite pores. Computational studies could be used to test these hypotheses and elucidate the changes in adsorbate configuration with respect to carbon number, zeolite topology, and number of hydroxyl groups.

Acknowledgment. The authors acknowledge the financial support from a Discovery Grant from the Institute on the Environment. Partial support for this work was also provided by the National Science Foundation: CBET 0855863. Dongxia Liu, Kumar Varoon, and Pyungsoo Lee synthesized the MCM-36, ITQ-1, and 3DOm-MFI materials, respectively. We thank Dr. Marc von Keitz for use of the HPLC. We also thank Joshua Kranz for assistance in the adsorption experiments. In memoriam: H. Ted Davis.

References and Notes

(1) Christensen, C. H.; Rass-Hansen, J.; Marsden, C. C.; Taarning, E.; Egeblad, K. *Chemsuschem* **2008**, *1*, 283.
(2) Petrus, L.; Noordermeer, M. A. *Green Chem.* **2006**, *8*, 861.
(3) Corma, A.; Iborra, S.; Velty, A. *Chem. Rev.* **2007**, *107*, 2411.
(4) Xiu, Z. L.; Zeng, A. P. *Appl. Microbiol. Biotechnol.* **2008**, *78*, 917–926.
(5) Caro, J.; Noack, M.; Kolsch, P.; Schafer, R. *Microporous Mesoporous Mater.* **2000**, *38*, 3.
(6) Corma, A.; Orchilles, A. V. *Microporous Mesoporous Mater.* **2000**, *35−6*, 21.
(7) Butler, A. C.; Nicolaides, C. P. *Catal. Today* **1993**, *18*, 443.
(8) Feller, A.; Lercher, J. A. *Adv. Catal.* **2004**, *48*, 229.
(9) Weitkamp, J.; Traa, Y. *Catal. Today* **1999**, *49*, 193.
(10) Eder, F.; Lercher, J. A. *Zeolites* **1997**, *18*, 75.
(11) Eder, F.; Lercher, J. A. *J. Phys. Chem. B* **1997**, *101*, 1273.
(12) Eder, F.; Stockenhuber, M.; Lercher, J. A. *J. Phys. Chem. B* **1997**, *101*, 5414.
(13) Denayer, J. F.; Baron, G. V.; Martens, J. A.; Jacobs, P. A. *J. Phys. Chem. B* **1998**, *102*, 3077.
(14) Denayer, J. F. M.; Ocakoglu, R. A.; Thybaut, J.; Marin, G.; Jacobs, P.; Martens, J.; Baron, G. V. *J. Phys. Chem. B* **2006**, *110*, 8551.
(15) Savitz, S.; Siperstein, F.; Gorte, R. J.; Myers, A. L. *J. Phys. Chem. B* **1998**, *102*, 6865.
(16) Denayer, J. F.; Souverijns, W.; Jacobs, P. A.; Martens, J. A.; Baron, G. V. *J. Phys. Chem. B* **1998**, *102*, 4588.
(17) Ison, A.; Gorte, R. J. *J. Catal.* **1984**, *89*, 150.
(18) Nakamoto, H.; Takahashi, H. *Zeolites* **1982**, *2*, 67.
(19) Mirth, G.; Lercher, J. A.; Anderson, M. W.; Klinowski, J. *J. Chem. Soc., Faraday Trans.* **1990**, *86*, 3039.
(20) Lee, C. C.; Gorte, R. J.; Farneth, W. E. *J. Phys. Chem. B* **1997**, *101*, 3811.
(21) Long, Y. C.; Jiang, H. W.; Zeng, H. *Langmuir* **1997**, *13*, 4094.
(22) Li, S.; Tuan, V. A.; Falconer, J. L.; Noble, R. D. *Microporous Mesoporous Mater.* **2002**, *53*, 59.
(23) Li, S. G.; Tuan, V. A.; Falconer, J. L.; Noble, R. D. *Chem. Mater.* **2001**, *13*, 1865.
(24) Li, S. G.; Tuan, V. A.; Falconer, J. L.; Noble, R. D. *Ind. Eng. Chem. Res.* **2001**, *40*, 1952.
(25) Li, S. G.; Tuan, V. A.; Falconer, J. L.; Noble, R. D. *J. Membr. Sci.* **2001**, *191*, 53.
(26) de Moor, P.; Beelen, T. P. M.; van Santen, R. A. *J. Phys. Chem. B* **1999**, *103*, 1639.
(27) Narkhede, V. V.; Gies, H. *Chem. Mater.* **2009**, *21*, 4339.
(28) Kruk, M.; Jaroniec, M.; Ko, C. H.; Ryoo, R. *Chem. Mater.* **2000**, *12*, 1961.
(29) Fan, W.; Snyder, M. A.; Kumar, S.; Lee, P. S.; Yoo, W. C.; McCormick, A. V.; Penn, R. L.; Stein, A.; Tsapatsis, M. *Nat. Mater.* **2008**, *7*, 984.
(30) Schmidt, I.; Madsen, C.; Jacobsen, C. J. H. *Inorg. Chem.* **2000**, *39*, 2279.
(31) Maheshwari, S.; Jordan, E.; Kumar, S.; Bates, F. S.; Penn, R. L.; Shantz, D. F.; Tsapatsis, M. *J. Am. Chem. Soc.* **2008**, *130*, 1507.
(32) He, Y. J.; Nivarthy, G. S.; Eder, F.; Seshan, K.; Lercher, J. A. *Microporous Mesoporous Mater.* **1998**, *25*, 207.
(33) Olson, D. H.; Haag, W. O.; Lago, R. M. *J. Catal.* **1980**, *61*, 390.
(34) Sano, T.; Kasuno, T.; Takeda, K.; Arazaki, S.; Kawakami, Y. Sorption of water vapor on HZSM-5 type zeolites In *Progress in Zeolite and Microporous Materials, Pts a−C*; Elsevier Science Publ B V: Amsterdam, 1997; Vol. 105, p 1771.
(35) Flanigen, E. M.; Bennett, J. M.; Grose, R. W.; Cohen, J. P.; Patton, R. L.; Kirchner, R. M.; Smith, J. V. *Nature* **1978**, *271*, 512.
(36) Marcolli, C.; Peter, T. *Atmos. Chem. Phys.* **2005**, *5*, 1545.
(37) Smit, B.; Maesen, T. L. M. *Nature* **1995**, *374*, 42.
(38) Vlugt, T. J. H.; Zhu, W.; Kapteijn, F.; Moulijn, J. A.; Smit, B.; Krishna, R. *J. Am. Chem. Soc.* **1998**, *120*, 5599.
(39) McCusker, C. B. a. L. B. Database of Zeolite Structures; http://www.iza-structure.org/databases/, 2007.
(40) Bates, S. P.; van Well, W. J. M.; van Santen, R. A.; Smit, B. *J. Phys. Chem.* **1996**, *100*, 17573.
(41) Ryoo, R.; Ko, C. H.; Kruk, M.; Antochshuk, V.; Jaroniec, M. *J. Phys. Chem. B* **2000**, *104*, 11465.
(42) Lukens, W. W.; Schmidt-Winkel, P.; Zhao, D. Y.; Feng, J. L.; Stucky, G. D. *Langmuir* **1999**, *15*, 5403.
(43) Pieterse, J. A. Z.; Veefkind-Reyes, S.; Seshan, K.; Lercher, J. A. *J. Phys. Chem. B* **2000**, *104*, 5715.
(44) Beerdsen, E.; Dubbeldam, D.; Smit, B.; Vlugt, T. J. H.; Calero, S. *J. Phys. Chem. B* **2003**, *107*, 12088.
(45) June, R. L.; Bell, A. T.; Theodorou, D. N. *J. Phys. Chem.* **1990**, *94*, 1508.
(46) Smit, B.; Loyens, L.; Verbist, G. Simulation of adsorption and diffusion of hydrocarbons in zeolites. *General Discussion Meeting on Solid State Chemistry - New Opportunities from Computer Simulations*; London, England, 1997.

JP910543R